2024 IEEE Intelligent Vehicles Symposium (IV)
June 2-5, 2024. Jeju Island, Korea

Fundamental Rules of Teleoperated Driving with Network Latency on Curvy Roads

Xunbi A. Ji, Sergei S. Avedisov, Mohammad Irfan Khan, M. Carmen Lucas-Estañ,
Baldomero Coll-Perales, Illés Vörös, Onur Altintas, and Gábor Orosz

2024 IEEE Intelligent Vehicle Symposium (IV) | 979-8-3503-4881-1/24/$31.00 ©2024 IEEE | DOI: 10.1109/IV55156.2024.10588495

***Abstract*— In this paper, we demonstrate how the network latency, the longitudinal velocity and the path curvature affect performance of the teleoperated driving (ToD). The performance of a ToD system is studied analytically through stability analysis of a dimensionless vehicle dynamics model with a scaled delay, which integrates the end-to-end (E2E) latency and the longitudinal velocity of the vehicle. We also establish a numerical simulation framework for ToD while incorporating a stochastic latency in the control loop arising from vehicle-to-network-to-vehicle (V2N2V) communication through a wireless network. The stochasticity of the latency mostly comes from the network scalability challenges to support high video bitrates, which also leads to packet drops. We provide simulation results of teleoperating a vehicle in a realistic parking lot scenario and demonstrate the effects of speed, curvature and stochastic latency on the maneuver performance.**

***Index Terms*— teleoperated driving, network latency, vehicle dynamics and control**

I. Introduction

As a supplement to automated driving [1], where vehicles control their motion using on-board computation units; teleoperated driving (ToD) has control commands given through a communication network [2], [3]. With ToD, the vehicles can offload the expensive computation units to reduce cost, while still enjoy the same (or even more) computational power, as well as the automated features provided by the remote operator center. Moreover, under emergency situations, such as system failure of the autonomous vehicle or medical emergency of the human driver, teleoperated vehicles allow the remote operator (either automated or human operated) to take over and ensure safety.

The architecture of a ToD control loop is presented in Fig. 1. The teleoperated vehicle sends the information of the surrounding environment to the remote controller via the uplink communication channel, and the remote center sends instructions back to the vehicle via the downlink communication channel for execution. One of the biggest challenges introduced by such a communication structure is the latency [4]–[6]. According to the standard SAE J3016 [7], depending on the type of instructions sent by the remote center and the autonomy level of the vehicle, the types of ToD can be categorized into three levels [8]: strategic level, tactical level, and operational level. In this paper, we focus on the operational level where the actual commands, such as velocity and steering angle, are sent to the vehicle instead of the high-level plans. One of the applications is valet parking, where the remote operator drives the vehicle in a parking lot at low speeds. This type of operation does not require high autonomy from the teleoperated vehicles, but it is sensitive to the latency experienced in the control loop.

The end-to-end (E2E) latency originates from multiple sources: (i) Time needed to send and receive data packets [5], [9]; (ii) Processing time of the remote operator [10]–[12]; (iii) Actuation delay of the vehicle [13], [14]. In addition, the increase of the latency can result in packet loss that strongly impacts the ToD service performance [5], [15]. While researchers and engineers have been working on designing low-latency communication networks and on reducing latency in video streaming [16], [17], the E2E latency cannot be eliminated due to the latency sources (ii)-(iii). For example, an automated vehicle can have a non-negligible delay in the longitudinal dynamics of around 0.6 seconds [18]. The E2E latency in the control loop also varies in time, due to the packet loss in the communication network and the zero-order-hold implementation of the control commands [5], [15]. The stochasticity in latency can sometimes lead to unstable behaviors even though the system is stable under its average latency [19]. It is crucial to account for the E2E latency when evaluating the controller's performance [20].

The contributions of this work are summarized as follows. First, we show that the E2E latency and the longitudinal velocity have the same fundamental effect on stability, which can be characterized by a scaled delay using a dimensionless vehicle dynamics model. Second, we derive the stability boundaries in closed form for different scaled delay and path curvature values, providing performance bounds for a given controller under different scenarios. Third, we consider stochastic network latencies in numerical simulations of realistic driving scenarios using a wireless network under different ToD network traffic conditions.

The rest of the paper is organized as follows. In Section II, we introduce the vehicle model and the control algorithm, and conduct stability analysis on the linearized and nondimensionalized vehicle dynamics model with constant E2E latency. Then, in Section III, we introduce a more realistic communication latency model and provide simulation results for ToD scenarios in a parking lot. We conclude the results and provide future directions in Section IV.

Xunbi A. Ji, Illés Vörös and Gábor Orosz are with the Department of Mechanical Engineering, University of Michigan, Ann Arbor, MI 48109, USA. {xunbij, illesvoe, orosz}@umich.edu.

Sergei S. Avedisov, Mohammad Irfan Khan, and Onur Altintas are with Toyota Motor North America R&D – InfoTech Labs, Mountain View, CA 94043, USA. {sergei.avedisov, mohammad.irfan.khan, onur.altintas}@toyota.com.

M. Carmen Lucas-Estañ, and Baldomero Coll-Perales are with Universidad Miguel Hernández de Elche, 03202 Elche, Alicante, Spain {m.lucas, bcoll}@umh.es.

Gábor Orosz is also with the Department of Civil and Environmental Engineering, University of Michigan, Ann Arbor, MI 48109, USA.

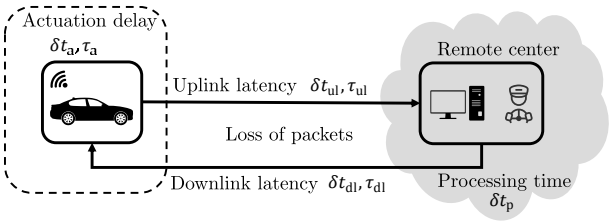

Fig. 1. Latency components in the control loop of teleoperated driving: δt_{ul} and δt_{dl} are the minimum sampling times in the uplink and downlink, respectively; τ_{ul} and τ_{dl} are the travel times in the uplink and downlink, respectively; δt_p is the processing time of the remote controller; δt_a is the minimum sampling time of the actuator; and τ_a is the actuation delay.

II. Stability Analysis with Constant Latency

The stability of the lateral vehicle dynamics when following a straight path with time delay was studied in [21] for both linear and nonlinear systems. In this work, we focus on the case of following a curved path. In this section, we establish the closed-loop dynamics of a vehicle model with time delay in the control loop while utilizing path coordinates, and analyze the stability of the linearized, nondimensionalized system.

A. Closed-loop Time Delay System

Consider the bicycle model of a vehicle [22] in Fig. 2, where v is the longitudinal velocity and l is the wheelbase. The center of the rear axle R has the coordinates (x_R, y_R), while the orientation of the vehicle is given by the yaw angle ψ, and γ denotes the steering angle. The dynamics of the vehicle is given by the differential equations

$$\begin{aligned} \dot{x}_R &= v\cos\psi, \\ \dot{y}_R &= v\sin\psi, \\ \dot{\psi} &= \frac{v}{l}\tan\gamma, \end{aligned} \tag{1}$$

where the dot represents the derivative with respect to time t.

The closest point to R along the path is point C, which is located at (x_C, y_C) and has the tangential angle ψ_C and the curvature κ. Thus, the lateral deviation from the path is defined as

$$\varepsilon = -(x_R - x_C)\sin\psi_C + (y_R - y_C)\cos\psi_C, \tag{2}$$

and the relative yaw angle is defined as

$$\theta = \psi - \psi_C. \tag{3}$$

With these coordinates, the model (1) can be formulated as

$$\begin{aligned} \dot{s} &= \frac{v\cos\theta}{1-\kappa\varepsilon}, \\ \dot{\varepsilon} &= v\sin\theta, \\ \dot{\theta} &= \frac{v}{l}\tan\gamma - \frac{v\kappa\cos\theta}{1-\kappa\varepsilon}, \end{aligned} \tag{4}$$

where s is the arclength at point C.

Inspired by the controller in [23], we use the controller

$$\gamma_d = \arctan\Big(l\kappa - k_1\big(\theta + \arctan(k_2\varepsilon)\big)\Big), \tag{5}$$

to assign the desired steering angle, where k_1, k_2 are the control gains.

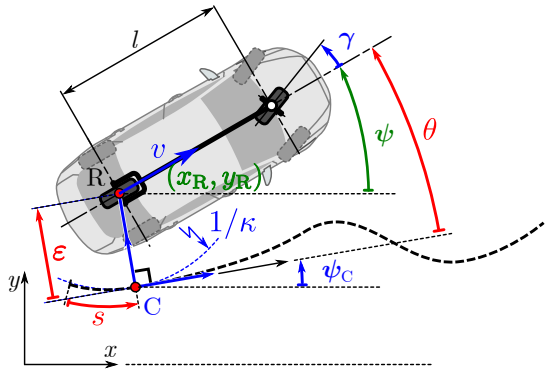

Fig. 2. Bicycle model of the vehicle represented in path coordinate system

In real-world implementations, the velocity and steering angle commands may not be achieved immediately due to the communication latency and neglected dynamics in acceleration and steering rate. Therefore time delays should be considered in the inputs. We assume that the vehicle can realize the desired velocity v_d and steering command γ_d with some delay, that is, $v(t) = v_d(t-\tau)$, $\gamma(t) = \gamma_d(t-\tau)$. Then the closed-loop system can be represented by the delay differential equations

$$\begin{aligned} \dot{s}(t) =& \frac{v_d(t-\tau)\cos\theta(t)}{1-\kappa(t)\,\varepsilon(t)}, \\ \dot{\varepsilon}(t) =& v_d(t-\tau)\sin\theta(t), \\ \dot{\theta}(t) =& -\frac{v_d(t-\tau)\kappa(t)\cos\theta(t)}{1-\kappa(t)\,\varepsilon(t)} + \frac{v_d(t-\tau)}{l}\Big(l\,\kappa(t-\tau) \\ & - k_1\Big(\theta(t-\tau) + \arctan\big(k_2\varepsilon(t-\tau)\big)\Big)\Big). \end{aligned} \tag{6}$$

Note that the curvature $\kappa(t)$ is time-varying because point C travels along the path as the vehicle moves. Moreover, the latency τ can also be a function of time. We will consider these factors in the numerical simulations in Section III.

B. Stability Analysis

For the stability analysis, we assume that the vehicle is running at a constant velocity $v(t) \equiv v_*$ while trying to approach a circular reference path of constant curvature $\kappa(t) \equiv \kappa_*$. The system (6) has a desired steady-state solution

$$s_*(t) = v_* t, \quad \varepsilon_*(t) \equiv 0, \quad \theta_*(t) \equiv 0. \tag{7}$$

By defining the perturbations $\tilde{s} = s - s_*$, $\tilde{\varepsilon} = \varepsilon - \varepsilon_*$, $\tilde{\theta} = \theta - \theta_*$, we can obtain the linearized system

$$\begin{aligned} \dot{\tilde{s}}(t) =& v_*\kappa_*\tilde{\varepsilon}(t), \\ \dot{\tilde{\varepsilon}}(t) =& v_*\tilde{\theta}(t), \\ \dot{\tilde{\theta}}(t) =& -v_*\kappa_*^2\tilde{\varepsilon}(t) - \frac{v_* k_1 k_2}{l}\tilde{\varepsilon}(t-\tau) - \frac{v_* k_1}{l}\tilde{\theta}(t-\tau). \end{aligned} \tag{8}$$

This can be nondimensionalized by using the scaled quantities $\hat{t} = t v_*/l$, $\hat{\tau} = \tau v_*/l$, $\hat{s} = \tilde{s}/l$, $\hat{\varepsilon} = \tilde{\varepsilon}/l$, $\hat{\theta} = \tilde{\theta}$:

$$\begin{aligned} \hat{s}'(\hat{t}) =& l\,\kappa_*\hat{\varepsilon}(\hat{t}), \\ \hat{\varepsilon}'(\hat{t}) =& \hat{\theta}(\hat{t}), \\ \hat{\theta}'(\hat{t}) =& -l^2\kappa_*^2\hat{\varepsilon}(\hat{t}) - k_1 k_2\, l\,\hat{\varepsilon}(\hat{t}-\hat{\tau}) - k_1\hat{\theta}(\hat{t}-\hat{\tau}), \end{aligned} \tag{9}$$

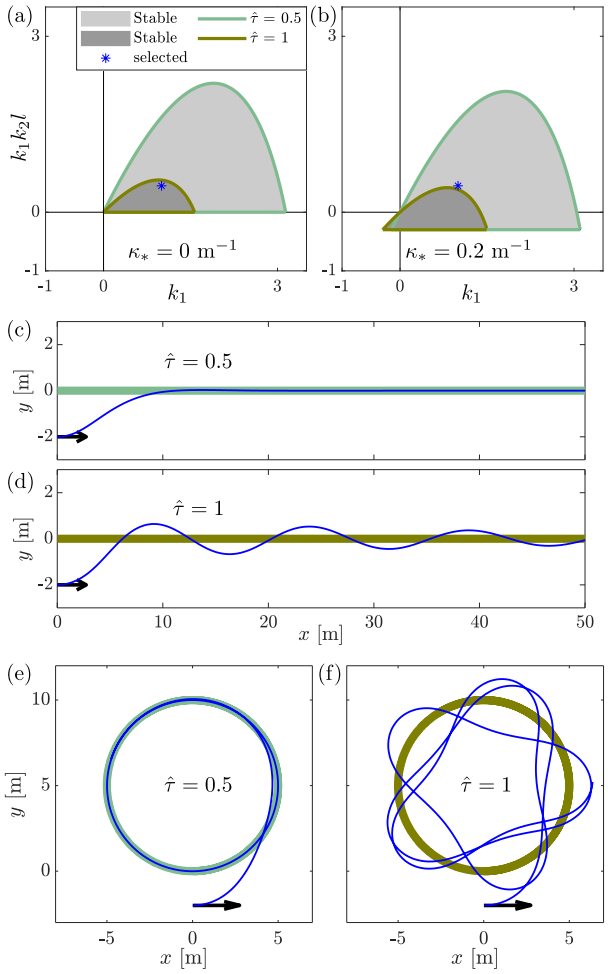

Fig. 3. (a)-(b) Stability charts for curvatures $\kappa_* = 0$ m^{-1} and $\kappa_* = 0.2$ m^{-1}. (c)-(d) Simulations when following a straight path ($\kappa_* = 0$ m^{-1}) under different scaled delays. (e)-(f) Simulations when following a circular path ($\kappa_* = 0.2$ m^{-1}) under different scaled delays.

where the prime represents the derivative with respect to the nondimensional time $\hat{t}$. Assuming exponential solutions results in the characteristic equation

$$\lambda^2 + k_1 \lambda \mathrm{e}^{-\lambda \hat{\tau}} + k_1 k_2 \, l \, \mathrm{e}^{-\lambda \hat{\tau}} + l^2 \kappa_*^2 = 0. \tag{10}$$

The linear system (9) is stable if and only if all characteristic roots of (10) have negative real parts, i.e., $\mathrm{Re}(\lambda_i) < 0, i = 1, 2, \ldots$. Substituting $\lambda = 0$ yields the stability boundary

$$k_1 k_2 l = -l^2 \kappa_*^2, \tag{11}$$

while using $\lambda = \mathrm{j}\omega$, $\omega > 0$, results in the stability boundary

$$\begin{aligned} k_1 &= (\omega^2 - l^2 \kappa_*^2) \frac{\sin(\omega \hat{\tau})}{\omega}, \\ k_1 k_2 l &= (\omega^2 - l^2 \kappa_*^2) \cos(\omega \hat{\tau}). \end{aligned} \tag{12}$$

which is parameterized by the angular frequency ω. Recall that the longitudinal velocity v_* is integrated with the latency τ in the scaled (dimensionless) delay $\hat{\tau} = \tau v_* / l$.

The stability boundaries of different scaled delays are plotted in Fig. 3(a) and (b) for curvatures $\kappa_* = 0$ m^{-1} and $\kappa_* = 0.2$ m^{-1}, respectively. The stable region shrinks as the scaled delay increases and increasing the curvature shifts the stable region downwards. In panels (c)-(f), we show the numerical simulations of the original nonlinear system (6) with gains $k_1 = 1, k_1 k_2 l = 0.45$, latency $\tau = 0.5$ s, and wheelbase $l = 2.73$ m while following a straight path ($\kappa_* = 0$ m^{-1}) and a 5-meter-radius circle ($\kappa_* = 0.2$ m^{-1}). The initial position and the orientation of the vehicle are visualized using black arrows. By choosing different velocities $v_* = 2.73$ m/s and $v_* = 5.46$ m/s, the scaled delays are $\hat{\tau} = 0.5$ and $\hat{\tau} = 1$, respectively. For $\hat{\tau} = 0.5$ the control gains are located within the stability boundary in panels (a)-(b) and the trajectories converge to the desired paths in panels (c) and (e). For zero curvature, as the scaled delay increases to $\hat{\tau} = 1$, the stability boundary gets close to the selected gains while still enclosing them in panel (a). This results in the oscillatory (but still stable) motion in panel (d). That is, increasing the scaled delay leads to performance degradation. For nonzero curvature, the same gains fall outside the stable region in panel (b) and simulations in panel (f) show that the system no longer converges to the circular path.

The performance of the controller is largely affected by the scaled delay, i.e., the longitudinal velocity and the E2E latency in the loop. The path curvature can also limit the performance in the presence of the latency. The stability analysis provides insights about the behavior of the original nonlinear system and informs us about the performance of a given controller for different maneuvers.

III. Numerical Simulation with Stochastic Time-varying Latency

In this section, we consider stochastic network latency in the control loop and use numerical simulations to examine the performance when teleoperating a vehicle which follows a curved path with a prescribed velocity profile. The E2E latency, the longitudinal velocity, and the path curvature are all time-varying in this scenario.

A. Model of Stochastic Time-varying Latency

We model different latencies in the control loop which constitute the E2E latency. We account for latencies arising from the transmission of the packets through the uplink and downlink channels of a mobile wireless network, from the processing time of the teleoperating center, and from the actuation time of the vehicle; see Fig. 1.

We consider a scenario where the ToD service is supported by a wireless network. In this case, the packets are sent from the vehicle to the remote center along the uplink every δt_{ul} (corresponding to the maximum sampling rate) and the travel time of each packet between the vehicle and remote center is τ_{ul}, see top of Fig. 4(a). The controller in the remote center has a processing delay δt_{p}. This is fixed such that it covers the time of converting the latest received images/information into the states of the system and the time of computing the control commands. During the processing time, the controller is not taking new information arriving at the remote center. A zero-order-hold (ZOH) is used to convert the command generated by the controller from discrete time to continuous

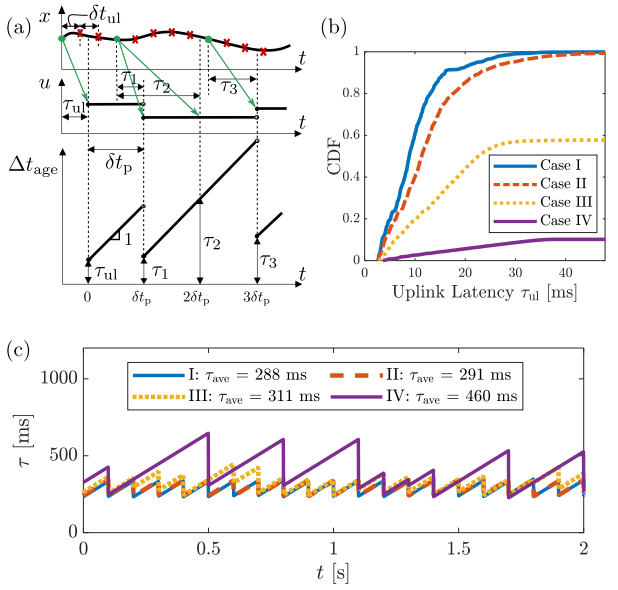

Fig. 4. (a) Age of information arising in the uplink due to the sampling time $\delta t_{\rm ul}$, travel time $\tau_{\rm ul}$, packet drops, and zero-order-hold in the controller. (b) The cumulative distribution function (CDF) of the travel time $\tau_{\rm ul}$ in the uplink. (c) The realizations of stochastically varying E2E latency profiles.

Case	Vehicle density	Image quality	Average uplink & downlink latencies $\langle\tau_{\rm ul}\rangle$ & $\langle\tau_{\rm dl}\rangle$	Packet drop ratio
I	Low[1]	Low[3]	9.90 ms & 8.41 ms	$< 0.1\%$
II	Low	High[4]	12.90 ms & 8.41 ms	0.2%
III	High[2]	Low	17.00 ms & 8.42 ms	42.3%
IV	High	High	24.14 ms & 8.42 ms	89.8%

[1] 1 veh/km/lane [2] 2 veh/km/lane [3] 4.5 Mbps [4] 32 Mbps

TABLE I

CHARACTERISTICS OF THE NETWORK LATENCY IN FOUR CASES

time, that is, the control inputs are held constant between two consecutive commands. This results in a linearly increasing latency until a new command is generated [24].

We define the age of information for the nth command as

$$\Delta t_{\rm age}(t_{{\rm C},n}) = t_{{\rm C},n} - t_{{\rm P},m}, \tag{13}$$

where $t_{{\rm C},n}$ is the time when the controller takes in the information, and $t_{{\rm P},m}$ is the time when the mth packet is sent from the vehicle. Here, the mth packet is the latest packet received at $t_{{\rm C},n}$, i.e., m can be viewed as a function of n. In Fig. 4(a), the controller is taking information every $\delta t_{\rm p}$ and $t_{{\rm C},n} = n\delta t_{\rm p}, n = 0, 1, 2, \ldots$. The packets are sent at $t_{{\rm P},m} = -\tau_{\rm ul} + m\delta t_{\rm p}, m = 0, 1, 2, \ldots$ via the uplink, so the first arrived packet triggers the controller at $t = 0$. Some packets are lost in the uplink, therefore one value of m could be associated to multiple values of n. The corresponding function $m(n)$ is stochastic and depends on the latency and packet drop ratio experienced in the uplink of the wireless network (modeled by the probabilistic network latency model). The age of information grows linearly with slope 1 between the generation of two commands. When the controller issues a new command, $\Delta t_{\rm age}(t)$ drops back to a lower value given by the time when the latest received packet was generated. This leads to the irregular saw-tooth-shape of the time-varying latency as shown in Fig 4(c) for four different cases.

After a control command is generated, it is sent through the downlink with minimum sampling time $\delta t_{\rm dl}$. The travel time in the downlink is $\tau_{\rm dl}$. The control commands are not dropped in the downlink since these are very small packets (compared to the video frames transmitted in the uplink), and thus, generate a small load on the network [5]. Once the vehicle receives the control command it executes it with minimum sampling time $\delta t_{\rm a}$ and subject to actuator delay $\tau_{\rm a}$ associated with the vehicle dynamics. Here, we assume that $\delta t_{\rm p}$ is the largest among $\delta t_{\rm ul}, \delta t_{\rm p}, \delta t_{\rm dl}, \delta t_{\rm a}$, i.e., the control commands are generated at a slower rate than other components. Consequently, the commands can always be sent immediately after generation and executed immediately after arriving at the vehicle. Therefore, the time at which the nth command is realized at the teleoperated vehicle is

$$t_n = t_{{\rm C},n} + \delta t_{\rm p} + \tau_{\rm dl} + \tau_{\rm a} = (n+1)\delta t_{\rm p} + \tau_{\rm dl} + \tau_{\rm a}, \tag{14}$$

and the E2E latency in control loop at t_n is

$$\tau(t_n) = t_n - t_{{\rm P},m(n)}. \tag{15}$$

In general for $t \in (t_n, t_{n+1})$, the E2E latency is given by

$$\tau(t) = t - t_n + \tau(t_n). \tag{16}$$

Considering the stochasticity of the communication networks, we use the probabilistic model [25] developed for four common scenarios defined based on the ToD service requirements established by 5GAA [26]. More details can be found in [6]. Figure 4(b) depicts the cumulative distribution function (CDF) of latency experienced in the uplink when packets are transmitted from the vehicle to the remote controller through the wireless network. Note that because some packets are dropped, the CDF does not always reach 1. The average uplink and downlink latencies and the packet drop ratios under these four different cases are collected in Table I.

To obtain the realistic latency profile as a function of time, we generate a sequence of packets at times $t_{{\rm P},m} = -\tau_{\rm ul} + m\delta t_{\rm ul}$ and use the probabilistic model to determine the latency for each packet and whether the packet is delivered or not. The uplink packet sequence will record the latest arrived packet number m versus time t. Thus, at time $t_{{\rm C},n}$, one can obtain the corresponding index m and the sending time of mth packet $t_{{\rm P},m} = m\delta t_{\rm ul}$. Every time when a command based a new packet is generated, we use the probabilistic network latency model to obtain the downlink latency $\tau_{\rm dl}$.

We use $\delta t_{\rm ul} = \delta t_{\rm dl} = \delta t_{\rm a} = 20$ ms [25], $\delta t_{\rm p} = 100$ ms, $\tau_{\rm a} = 100$ ms as constants, and $\tau_{\rm ul}, \tau_{\rm dl}$ as random variables whose values are sampled from the network latency model. The E2E latency profiles as a function of time can then be generated using (14)-(16). The realizations of latency profiles in four common cases are shown in Fig. 4(c) with their

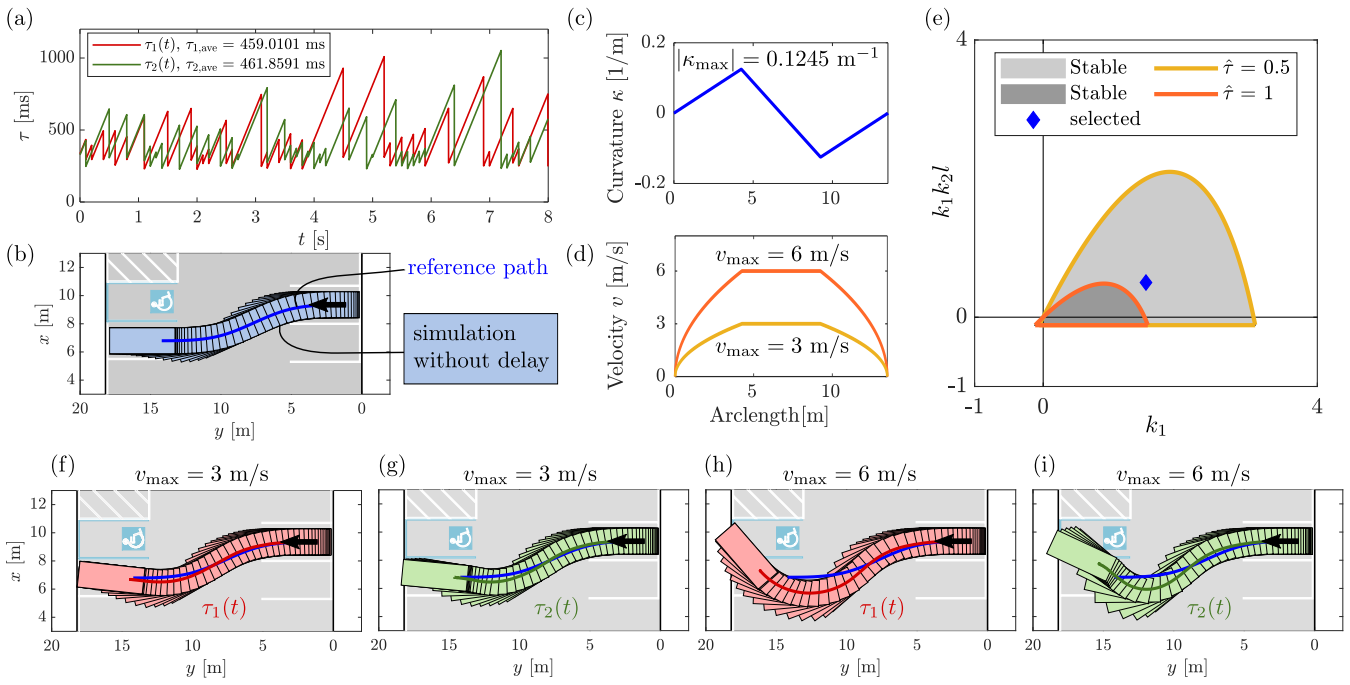

Fig. 5. Simulation results for different latency profiles and velocity plans. (a) Two latency profiles generated based on Case IV, $\tau_{\text{ave}} = 0.46$ s. (b) Reference path (blue solid curve) and the simulation of the ToD without any latency. (c) The curvature function along the reference path with $|\kappa_{\max}| = 0.1245$ m^{-1}. (d) Two velocity plans along the given path with $v_{\max} = 3$ m/s or $v_{\max} = 6$ m/s. (e) Stability chart for $\kappa_* = 0.1245$ m^{-1}, $\tau = 0.46$ s, $v_* = 3$ m/s $\Rightarrow \hat{\tau} = 0.5$, and $\tau = 0.46$ s, $v_* = 6$ m/s $\Rightarrow \hat{\tau} = 1$. (f)-(i) Simulation results for the different velocity plans, with latency profiles $\tau_1(t)$ (red) and $\tau_2(t)$ (green) respectively.

average values τ_{ave} highlighted. When the packet drop ratio is low, the stochasticity in $\tau_{\text{ul}}, \tau_{\text{dl}}$ does not contribute much to the E2E latency. In these cases, the saw-tooth-shape profiles are more regular and can be approximated as a constant by taking the average of the latency. When the packet drop ratio is high, information loss can happen frequently in the uplink which affects the generation of new commands. Due to the stochasticity, the realizations of the E2E latency profiles can look very different for the same packet drop ratio, see Fig. 5(a).

B. Simulation Results

We present simulation results of ToD under stochastic time-varying latency for a parking lot scenario. The map of the parking lot is generated from measurements of a real lot. Here the vehicle's goal is to go from one parking spot to another following a given curved path, see Fig. 5. This case can be generalized to many low-speed maneuvers with predefined curvatures and velocity plans along the desired paths. The two stochastic latency profiles shown in panel (a) are generated for Case IV network configuration with average E2E latency $\tau_{\text{ave}} = 0.46$ s. This case is chosen since the effects of the stochastic latency are more pronounced due to the high packet drop ratio. We also conducted numerical simulations under other stochastic latency profiles generated for Cases I-III. In those cases the simulations are very similar to the simulations generated when using the average E2E latency as a deterministic delay. The vehicle starts from standstill at a spot on the right and terminates its motion at the spot on the left following the blue path in panel (b), with two different velocity plans. The desired path is determined by a continuous curvature function shown in panel (c), using the 3-clothoid method [27], [28]. The maximum curvature of the path is $\kappa_{\max} = 0.1245$ m^{-1} and the maximum velocities for the two velocity plans are $v_{\max} = 3$ m/s and $v_{\max} = 6$ m/s, as depicted in panel (d). When there is no latency in the teleoperated control loop, the vehicle can follow the path perfectly for both velocity profiles, see the light blue simulation in the panel (b).

The stability boundaries for constant curvature $\kappa_* = 0.1245$ m^{-1}, constant scaled delays $\hat{\tau} = 0.5$ and $\hat{\tau} = 1$ are shown in panel (e). The two scaled delays correspond to the same latency $\tau = 0.46$ s, wheelbase $l = 2.73$ m, but different velocities $v_* = 3$ m/s and $v_* = 6$ m/s. We choose the control gains $k_1 = 1.5$, $k_1 k_2 l = 0.5$ in the controller (5) as indicated by blue diamond, which is inside the stable region for $\hat{\tau} = 0.5$ but outside the stable region of $\hat{\tau} = 1$. We simulate the nonlinear closed-loop system (6) with time-varying $\tau(t)$, $v(t)$ and $\kappa(t)$. The simulation results for $v_{\max} = 3$ m/s are shown in panels (f) and (g), with the latency profiles $\tau_1(t)$ and $\tau_2(t)$, respectively. The difference between the vehicle trajectories is small in these two simulations. On the contrary, the simulations for the larger velocity $v_{\max} = 6$ m/s look very different in panels (h) and (i), which means that this maneuver is more sensitive to the stochasticity in the latency profiles. The linear stability analysis for the constant parameters (E2E latency, longitudinal velocity and path curvature) still provides useful insights regarding the qualitative results of the nonlinear simulations with time-varying parameters.

IV. Conclusion

We presented the effects of network latency, longitudinal velocity and path curvature on the performance of teleoperated driving (ToD) through both analytical investigation and numerical simulations. By rescaling the corresponding equations of motion, we derived the scaled delay parameter which captures the effects of both delay and speed on the stability of ToD. We showed how the scaled delay and the path curvature fundamentally change the stability of the ToD model. In the numerical simulations, we considered low-speed parking lot maneuvers where the teleoperated vehicle's goal was to move from one parking space to another. We accounted for the stochastic nature of wireless communication and obtained time-varying latency profiles by generating sequential packets using a realistic network latency model. Paths with larger curvature and higher speed profiles are more sensitive to the stochasticity of the network latency and the performance degrades as the average latency, the speed, or the curvature increases. The results based on the scaled delay also suggest that the remote operator shall lower the velocity if large latency is observed.

In this study, the perception and planning units were lumped into the controller with one processing delay. As a future direction, it is important to consider the effects of network latency on the accuracy of the state observations and the effects on the remote human operator's driving behaviors. Moreover, we plan to establish other metrics for evaluating the performance of ToD under network latency, considering the deviation from the path and the safety with respect to the surrounding environment. More sophisticated planning and control methods can be developed based on such evaluation.

Acknowledgment

We genuinely thank Javier Gozalvez and Miguel Sepulcre for sharing their insights on this work.

References

[1] T. Ersal, I. Kolmanovsky, N. Masoud, N. Ozay, J. Scruggs, R. Vasudevan, and G. Orosz, "Connected and automated road vehicles: state of the art and future challenges," *Vehicle System Dynamics*, vol. 58, no. 5, pp. 672–704, 2020.

[2] L. Kang, W. Zhao, B. Qi, and S. Banerjee, "Augmenting self-driving with remote control: Challenges and directions," in *19th International Workshop on Mobile Computing Systems & Applications*, 2018, pp. 19–24.

[3] R. Liu, D. Kwak, S. Devarakonda, K. Bekris, and L. Iftode, "Investigating remote driving over the lte network," in *9th International Conference on Automotive User Interfaces and Interactive Vehicular Applications*, 2017, pp. 264–269.

[4] S. Neumeier, P. Wintersberger, A.-K. Frison, A. Becher, C. Facchi, and A. Riener, "Teleoperation: The holy grail to solve problems of automated driving? Sure, but latency matters," in *11th International Conference on Automotive User Interfaces and Interactive Vehicular Applications*, 2019, pp. 186–197.

[5] M. C. Lucas-Estañ, B. Coll-Perales, I. K. Khan, S. S. Avedisov, O. Altintas, J. Gozalvez, and M. Sepulcre, "Support of teleoperated driving with 5G networks," in *98th IEEE Vehicular Technology Conference (VTC2023-Fall)*. IEEE, 2023, pp. 1–6.

[6] 5GCroco, "First phase trial execution report and analysis of 5gcroco kpi," *Deliverable D4.2v3.0*, 2021.

[7] S. International. Taxonomy and definitions for terms related to driving automation systems for on-road motor vehicles. [Online]. Available: https://www.sae.org/standards/content/j3016_202104/

[8] M.-P. Pacaux, S. D. Godin, B. Rajaonah, F. Anceaux, and F. Vanderhaegen, "Levels of automation and human-machine cooperation: Application to human-robot interaction," *IFAC Proceedings*, vol. 44, no. 1, pp. 6484–6492, 2011.

[9] Q. Yang and J. H. Yang, "Hd video transmission of multi-rotor unmanned aerial vehicle based on 5G cellular communication network," *Computer Communications*, vol. 160, pp. 688–696, 2020.

[10] G. L. Oliveira, W. Burgard, and T. Brox, "Efficient deep models for monocular road segmentation," in *IEEE/RSJ International Conference on Intelligent Robots and Systems (IROS)*. IEEE, 2016, pp. 4885–4891.

[11] S. D. Pendleton, H. Andersen, X. Du, X. Shen, M. Meghjani, Y. H. Eng, D. Rus, and M. H. Ang, "Perception, planning, control, and coordination for autonomous vehicles," *Machines*, vol. 5, no. 1, p. 6, 2017.

[12] J. Fayyad, M. A. Jaradat, D. Gruyer, and H. Najjaran, "Deep learning sensor fusion for autonomous vehicle perception and localization: A review," *Sensors*, vol. 20, no. 15, p. 4220, 2020.

[13] D. Yanakiev, J. Eyre, and I. Kanellakopoulos, "Analysis, design, and evaluation of AVCS for heavy-duty vehicles with actuator delays," *UC Berkeley: California Partners for Advanced Transportation Technology*, 1998. [Online]. Available: https://escholarship.org/uc/item/931877r2

[14] A. Nahidi, A. Khajepour, A. Kasaeizadeh, S.-K. Chen, and B. Litkouhi, "A study on actuator delay compensation using predictive control technique with experimental verification," *Mechatronics*, vol. 57, pp. 140–149, 2019.

[15] W. B. Qin and G. Orosz, "Scalable stability analysis on large connected vehicle systems subject to stochastic communication delays," *Transportation Research Part C*, vol. 83, pp. 39–60, 2017.

[16] Y. Yu and S. Lee, "Remote driving control with real-time video streaming over wireless networks: Design and evaluation," *IEEE Access*, vol. 10, pp. 64 920–64 932, 2022.

[17] O. El Marai and T. Taleb, "Smooth and low latency video streaming for autonomous cars during handover," *IEEE Network*, vol. 34, no. 6, pp. 302–309, 2020.

[18] X. A. Ji, T. G. Molnár, A. A. Gorodetsky, and G. Orosz, "Bayesian inference for time delay systems with application to connected automated vehicles," in *IEEE International Intelligent Transportation Systems Conference (ITSC)*. IEEE, 2021, pp. 3259–3264.

[19] H. T. Sykora, M. Sadeghpour, J. I. Ge, D. Bachrathy, and G. Orosz, "On the moment dynamics of stochastically delayed linear control systems," *International Journal of Robust and Nonlinear Control*, vol. 30, no. 18, pp. 8074–8097, 2020.

[20] P. Ghorai, A. Eskandarian, and Y.-K. Kim, "Study the effect of communication delay for perception and collision avoidance in cooperative autonomous driving," in *ASME International Mechanical Engineering Congress and Exposition*, vol. 84553. American Society of Mechanical Engineers, 2020, p. V07BT07A015.

[21] I. Vörös, G. Orosz, and D. Takács, "On the global dynamics of path-following control of automated passenger vehicles," *Nonlinear Dynamics*, vol. 111, no. 9, pp. 8235–8252, 2023.

[22] D. J. Limebeer and M. Massaro, *Dynamics and optimal control of road vehicles*. Oxford University Press, 2018.

[23] W. B. Qin, Y. Zhang, D. Takács, G. Stépán, and G. Orosz, "Nonholonomic dynamics and control of road vehicles: moving toward automation," *Nonlinear Dynamics*, vol. 110, no. 3, pp. 1959–2004, 2022.

[24] T. G. Molnár, W. B. Qin, T. Insperger, and G. Orosz, "Application of predictor feedback to compensate time delays in connected cruise control," *IEEE Transactions on Intelligent Transportation Systems*, vol. 19, no. 2, pp. 545–559, 2018.

[25] B. Coll-Perales, M. C. Lucas-Estañ, T. Shimizu, J. Gozalvez, T. Higuchi, S. Avedisov, O. Altintas, and M. Sepulcre, "End-to-end v2x latency modeling and analysis in 5G networks," *IEEE Transactions on Vehicular Technology*, vol. 72, no. 4, pp. 5094–5109, 2023.

[26] G. A. Association *et al.*, "Tele-operated driving (tod): Use cases and technical requirements," *5GAA Automotive Association, Tech. Rep*, 2021.

[27] E. Bertolazzi and M. Frego, "On the g2 hermite interpolation problem with clothoids," *Journal of Computational and Applied Mathematics*, vol. 341, pp. 99–116, 2018.

[28] S. Oh, Q. Chen, H. E. Tseng, G. Pandey, and G. Orosz, "Sharable motion planning for connected automated vehicles," in *International Symposium on Advanced Vehicle Control (AVEC)*, 2022.